Check for updates

L-Cysteine assisted-synthesis of 3D In₂S₃ for 3D CuInS₂ and its application in hybrid solar cells

Wenjin Yue, [iD] *[a] Feiyu Wei,[a] Chenbin He,[a] Dandan Wu,[a] Nengwen Tang[a] and Qiquan Qiao*[b]

In this paper, the L-cysteine assisted-synthesis of 3D In₂S₃ for 3D CuInS₂ with a walnut-shape structure was reported and the 3D CuInS₂ was applied in hybrid solar cells (HPSCs) for the first time. In the first step, 3D In₂S₃ was synthesized *via* a solvothermal method, with L-cysteine as the sulphur source, forming uniform flowerlike hierarchical structures. In the second step, chalcopyrite 3D CuInS₂ with a walnut-shape hierarchical structure was produced, using 3D In₂S₃ as the template and with the corporation of Cu²⁺. Correlated factors in the reaction, such as the molar quantity of L-cysteine and the solvent, were adjusted to study the formation process of 3D CuInS₂. 3D CuInS₂ displayed a wide absorption range in UV-vis spectra and quenched the fluorescence of poly(2-methoxy-5-(2-ethylhexyloxy)-1,4-phenylene vinylene) (MEH–PPV) effectively; therefore, it was applied to the fabrication of MEH–PPV/3D CuInS₂ solar cells, with a mixture of polymer and 3D CuInS₂ as the photoactive layer, for the first time, obtaining a PCE of 0.4% and confirming that 3D CuInS₂ could be applied in HPSCs successfully.

1. Introduction

Compared to commonly used energy sources, solar energy is non-polluting, renewable, and non-exhaustible; however, it is not in widespread use, owing to its expensive cost. Organic–inorganic hybrid polymer solar cells (HPSCs) are low-cost in the material synthesis, processable and versatile in the device manufacture, which has become attractive recently.[1] Normally, HPSCs with a bulk heterojunction are based on different inorganic nanoparticles such as ZnO,[2] TiOₓ,[3] CdSe,[4] CdS,[5] PbS,[6] PbSe[7] and CuInS₂.[8] The ternary compound CuInS₂, with a band gap of 1.5 eV (ref. 9) and an absorption coefficient of 10^5 cm⁻¹,[10] is an ideal material for efficient solar cells;[11] it exhibits good radiation stability, and it's easy to adjust the stoichiometry to obtain different conductivity (p-type or n-type).[12] Previously, we synthesized CuInS₂ quantum dots (QDs) and applied these in HPSCs, confirming that they are an effective electron acceptor for HPSCs with a wide spectral response over the range of 300–900 nm.[13]

It's well-known that the morphology of nanomaterials is one of the key factors affecting their properties. Nanostructures with novel morphologies have been considerably investigated. A 3D hierarchical structured material, which is assembled in an orderly manner from one or two nanoscale dimensions, has a large surface area and capacious interspaces, which could

provide more opportunities for polymer molecules to diffuse and transport effectively.[14] It would be of benefit for solar energy utilization, being obviously superior to 1D nanorods consisting of a low internal surface area.[15] In addition, it maintains the advantages of nanorods, and could afford a direct electron transport path in the case of the main junction remaining epitaxial.[16] These advantages make 3D structured materials a candidate for use in highly efficient solar cells. However, to the best of our knowledge, there are few reports on HPSCs based on 3D CuInS₂. In this paper, we fabricated HPSCs based on polymers and 3D CuInS₂.

First of all, the controllable synthesis of 3D CuInS₂ is important. Many efforts have been devoted to preparing 3D CuInS₂ in recent years.[17] It is well-known that the controlled synthesis of a 3D hierarchical structure of a ternary sulfide is more complicated than that of a binary sulfide. Template synthesis through cation exchange may provide a convenient and effective approach for constructing ternary or quaternary sulfide hierarchical architectures from the respective binary nanocrystals.[18] CuInS₂ is a ternary compound assembled from binary compounds such as CuS and In₂S₃, which makes the template synthesis of CuInS₂ from CuS or In₂S₃ feasible. Previously, Xie group and Zhu group synthesized CuInS₂ *in situ*, with CuS as the template.[19] However, the formation of CuInS₂ from In₂S₃ is energetically favourable compared to the use of a CuS precursor template.[20] Lei *et al.* fabricated CuInS₂ nanoparticles using a solvothermal method on the basis of micrometer-sized spinel In₃₋ₓS₄ templates,[21] and Chen *et al.* synthesized CuInS₂ nanocrystals using a template synthesis method with the incorporation of Cu⁺ cations into In₂S₃

[a]School of Biochemical Engineering, Anhui Polytechnic University, Wuhu, 241000, P. R. China. E-mail: yuewenjin_79@163.com

[b]Centre for Advanced Photovoltaics, Department of Electrical Engineering and Computer Sciences, South Dakota State University, Brookings, SD, 57007, USA. E-mail: Qiquan.Qiao@sdstate.edu

nanoplates.[22] However, there are few reports on the synthesis of 3D $CuInS_2$ with 3D In_2S_3 as the template, even though the binary 3D hierarchical structure exhibits unique properties in the structural evolution of the ternary 3D hierarchical structure. In_2S_3 is a III–VI group semiconductor with a bandgap of 2.0–2.3 eV; it normally exists in three different crystal phases: defective cubic structured α-In_2S_3, defective spinel structured β-In_2S_3 and layered hexagonal structured γ-In_2S_3.[23] In these three structures, β-In_2S_3 is the most stable. As a result, in this study, 3D β-In_2S_3 has been synthesized first.

However, to synthesize 3D In_2S_3, different factors would impact on the morphology of In_2S_3, such as the additive, reaction temperature, and reaction time. Particularly, the additive is the most important factor. Biomolecular additives have been widely used to synthesize different nanomaterials owing to their particular structures and attractive self-assembly functions, for instance, in the synthesis of snowflake-like Bi_2S_3,[24] Cu_2O dendrites,[25] CdS nanorod arrays[26] and other nanomaterials.[27] Considered as one of the most important types of biomolecules, amino acids have drawn much attention in recent years. In particular, L-cysteine, an amino acid that contains the thiol group, can normally be used as an additive in the synthesis of metal sulfides, such as in the synthesis of flower-like In_2S_3,[28] pagoda-like hierarchical PbS,[29] NiS microcrystals,[30] Sb_2S_3 microspheres,[31] Ag_2S nanospheres,[32] 3D structured ZnS[33] and CdS nanospheres.[34] It could be observed that, in these reactions, L-cysteine is normally used in a one-step reaction to synthesize just one product. In this paper, we used L-cysteine separately in the synthesis of 3D In_2S_3 and 3D $CuInS_2$, with the observation that 3D In_2S_3 impacts on the 3D $CuInS_2$ morphology, obtaining the evolutionary processes of the crystal phase and morphology from 3D In_2S_3 to 3D $CuInS_2$. Finally, solar cells based on polymers and synthesized 3D $CuInS_2$ were fabricated.

2. Materials and methods

2.1 Materials

Indium chloride tetrahydrate ($InCl_3 \cdot 4H_2O$, AR), copper(II) chloride dihydrate ($CuCl_2 \cdot 2H_2O$, AR), L-cysteine (biochemical reagent), thiourea (AR), N,N-dimethyl-formamide (DMF, AR), absolute glycol (AR), absolute ethanol (AR) and chlorobenzene (CP) were purchased from the Sinopharm Chemical Reagent Co, Ltd. MEH–PPV (M_n = 40 000–70 000, Aldrich), PEDOT:PSS (Clevios P HC V4, H. C. Starck) and lithium fluoride (LiF) (Alfa Aesar, 99.99%) were commercially obtained. The use of chlorobenzene was carried out after distillation under reduced pressure.

2.2 Synthesis of 3D In_2S_3

$InCl_3 \cdot 4H_2O$ (1 mmol) and 4.5 mmol of L-cysteine were dissolved in 40 mL of deionized water with stirring for 5 min, followed by an adjustment of the pH to 8, then were transferred into a Teflon-lined stainless steel autoclave and maintained at 180 °C for 12 h. After the autoclave naturally cooled to room temperature, the product was collected via centrifugation (16 000–20 000 rpm, 10 min), washed several times with

absolute ethanol and dried under vacuum at 60 °C for 6 h to obtain a yellow power. For comparison, thiourea was used instead of L-cysteine to carry out the same procedure.

2.3 Synthesis of 3D $CuInS_2$

Similar to the above procedure, 1 mmol of $InCl_3 \cdot 4H_2O$ and different molar quantities of L-cysteine (1.5 mmol, 3 mmol, 4.5 mmol and 6 mmol) were used to synthesize In_2S_3. 0.5 mmol In_2S_3, with the addition of 1 mmol of $CuCl_2 \cdot 2H_2O$ and 1 mmol of L-cysteine, was dissolved in 40 mL of deionized water, glycol or DMF, respectively; then the mixture was transferred into a Teflon-lined stainless steel autoclave and maintained at 180 °C for 24 h. Finally, the product was centrifuged, washed and dried.

2.4 Construction of solar cells

HPSCs were fabricated using a mixture containing MEH–PPV and the synthesized 3D $CuInS_2$ as the photoactive layer. Firstly, on an indium tin oxide (ITO) substrate (≤ 15 Ω Å^{-1}, Shenzhen Laibao Hi-Tech Co., Ltd, China), a PEDOT:PSS suspension passed through a 0.8 μm filter was spin-coated under ambient conditions, and dried at 140 °C for 30 min, obtaining a PEDOT:PSS layer. Then, an MEH–PPV/3D $CuInS_2$ photoactive layer was spin-coated on the PEDOT:PSS layer, with an MEH–PPV content of 5 mg mL^{-1} and a 3D $CuInS_2$ content of 5 mg mL^{-1} in chlorobenzene. Finally, a 100 nm Al film was deposited onto the photoactive layer, with a 1.0 nm LiF layer previously produced via thermal evaporation. The devices were sealed in a glovebox with the content of O_2 and H_2O at less than 1 ppm.

2.5 Characterization

Scanning electron microscopy (SEM) and transmission electron microscopy (TEM) observations were carried out on an FEI Sirion 200 microscope and a JEOL-2010 transmission electron microscope, respectively. Power X-ray diffraction (XRD) patterns were measured on an MXP18AHF X-ray diffractometer with monochromated Cu-Kα radiation (λ = 1.54056 Å). X-ray photoelectron spectroscopy (XPS) analyses were performed on an ESCALAB 250 XPS, using Al K_α X-rays as the excitation source, and all peaks were calibrated with C 1s (284.60 eV) as the reference. Raman spectra were obtained with the Renishaw inVia Raman spectrometer, using a 514 nm argon ion laser as the excitation source.

For optical measurements, MEH–PPV (at a concentration of 5 mg mL^{-1} in chlorobenzene) and MEH–PPV–$CuInS_2$ composited film (with MEH–PPV and $CuInS_2$ both at 5 mg mL^{-1} in chlorobenzene) were spin-coated on cleaned quartz substrates at 1500 rpm for 60 s. Absorption spectra were recorded on a UV 2550 spectrophotometer (Shimadzu), while photoluminescence (PL) spectra were measured on a F-7000 spectrofluorometer (Hitachi) with excitation at 480 nm. Before the optical measurements, all the films were kept under vacuum overnight at room temperature.

The current–voltage (J–V) curves were characterized using controlled intensity modulated photo-spectroscopy (CIMPS) (Zahner Co., Germany), with a blue light-emitting diode (LED)

as the light source. The effective illumination area of a cell was 0.04 cm^2 and Al was taken as the negative electrode, similarly to previous reports.[13a] The light was illuminated through the ITO glass side.

3.   Results and discussion

3.1   Synthesis of 3D In$_2$S$_3$

3.1.1   Morphology of 3D In$_2$S$_3$. Fig. 1 displays the morphology of In$_2$S$_3$ synthesized with different sulfur sources. Fig. 1a shows the morphology of In$_2$S$_3$ synthesized with thiourea as the sulfur source. It displays a spherical structure with a size of 600–700 nm, and is composed of tiny nanosheets like a tomentum on the surface. However, after the addition of L-cysteine, an SEM image (Fig. 1b) shows that uniform 3D flowerlike structures of about 500 nm appear on a large scale, with the nanosheets interleaving and slightly bending to form the petals. In a TEM image (shown in Fig. 1c), the flowerlike structures could be seen clearly, assembled from nanoflakes with a thickness of 10–20 nm. Obviously, the presence of L-cysteine could promote the formation of hierarchical 3D flower-like In$_2$S$_3$.

3.1.2   XRD analysis of In$_2$S$_3$. The phase structures of the products were characterized using powder X-ray diffraction (XRD). Fig. 2 shows the XRD pattern of the product synthesized with L-cysteine as the additive. Diffraction peaks at 2θ values of 21.9°, 27.4°, 28.6°, 32.3° and 47.7° matching with the (008), (109), (206), (208) and (2212) crystal planes of tetragonal β-In$_2$S$_3$ ($a = 7.619$ Å, $c = 32.329$ Å, JCPDS PCPDFWIN #25-0390) could be

observed. The XRD pattern confirmed the formation of In$_2$S$_3$ without the characteristic peaks of other impurities such as InS, In, and S, implying that a pure In$_2$S$_3$ phase could be synthesized successfully with L-cysteine as the additive.

3.1.3   XPS analysis of In$_2$S$_3$. XPS spectra were used to characterize the product composition more accurately, as shown in Fig. 3. From the survey spectrum (Fig. 3a), the existence of In, S, C and O could be inferred. C, at a high concentration, probably originated from L-cysteine residue covering the surface of In$_2$S$_3$, and the presence of O may be owed to atmospheric contamination of the sample. The valence state and atomic ratio of In to S could be obtained from the In 3d and S 2p spectra, respectively. There are two peaks located at 444.6 eV and 452.2 eV in the In 3d spectrum (shown in Fig. 3b), which correspond to In 3d$_{5/2}$ and In 3d$_{3/2}$,[28] respectively. The spin–orbit separation of In is 7.6 eV, indicating that In was present in the form of In^{3+}. In the S 2p spectrum (shown in Fig. 3c), two peaks at 161.35 eV and 162.55 eV could be seen, corresponding to S 2p$_{3/2}$ and S 2p$_{1/2}$, respectively.[35] The spin orbit separation of 1.2 eV suggested that S existed as S^{2-} in In$_2$S$_3$.[35,36] The ratio of In to S is estimated to be 1 : 1.5, in accordance with the stoichiometric ratio in In$_2$S$_3$.

3.2   Synthesis of 3D CuInS$_2$

3.2.1   Morphology of CuInS$_2$

3.2.1.1   The influence of the molar quantity of L-cysteine. Different morphologies of CuInS$_2$ are shown in Fig. 4. They were synthesized with 3D In$_2$S$_3$ as the template, while the 3D In$_2$S$_3$ was obtained with different molar quantities of L-cysteine as the additive. When the molar quantity of L-cysteine is very low, only some irregular shaped crystals with a very small size in the large matrix could be seen (Fig. 4a). When the molar quantity of L-cysteine was increased to 3.0 mmol, some small hierarchical structured crystals with a size of no more than 100 nm could be seen; the hierarchical structure is assembled from nanosheets (Fig. 4b). When the molar quantity was increased to 4.5 mmol, a large sized 3D hierarchical walnut-shape structure of 400–500 nm formed, which is assembled from nanosheets (Fig. 4c), similarly to Fig. 4b. However, when the molar quantity was
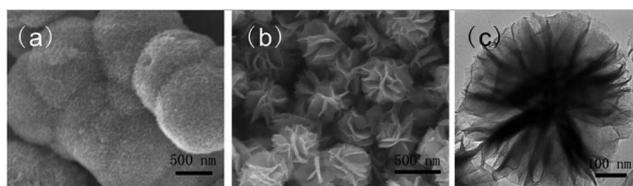

Fig. 1 SEM (a, b) and TEM (c) images of In$_2$S$_3$ with thiourea (a) and L-cysteine (b, c) as the additive.

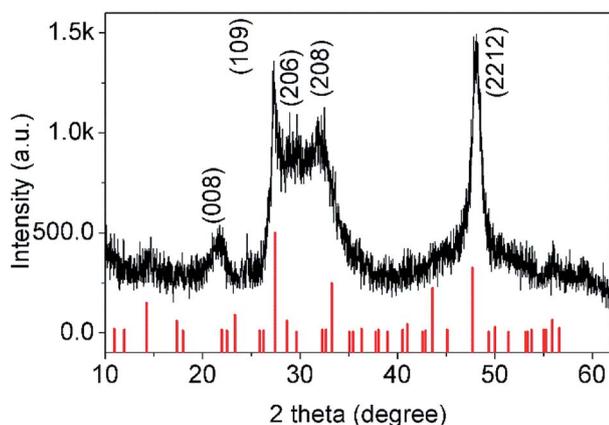**Fig. 2** XRD pattern of the as-synthesized In$_2$S$_3$.

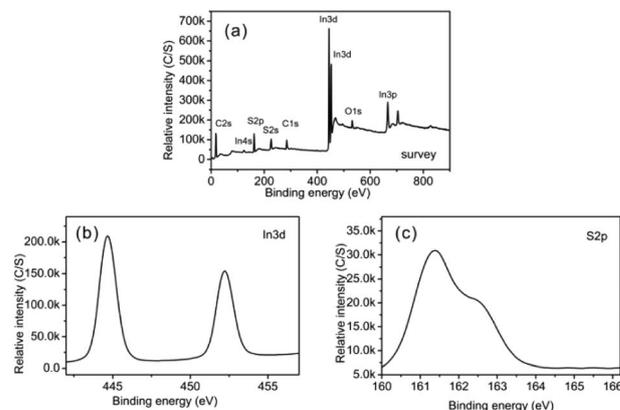**Fig. 3** XPS spectra of the as-synthesized In$_2$S$_3$: (a) a survey spectrum, (b) an In 3d spectrum, and (c) a S 2p spectrum.
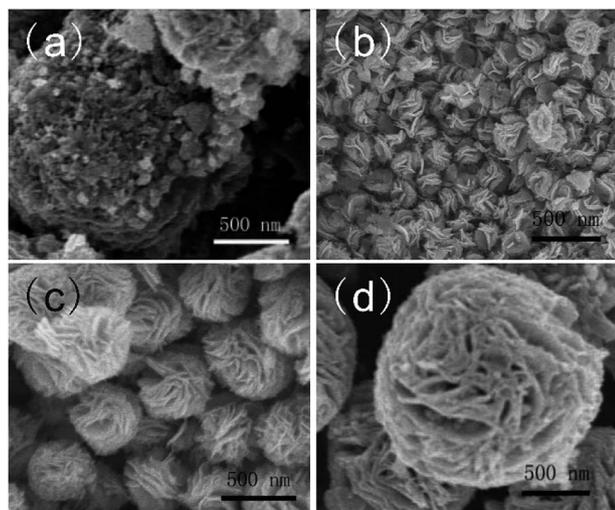
Fig. 4 SEM images of CuInS$_2$ synthesized with a molar quantity of L-cysteine of 1.5 mmol (a), 3.0 mmol (b), 4.5 mmol (c) and 6.0 mmol (d).

increased to 6.0 mmol, huge sized micrometer spheres formed with a size of 2–4 μm, but there are some small crystals adhering to the surface of the microspheres (Fig. 4d). Clearly, the molar quantity of L-cysteine played an important role in the formation of In$_2$S$_3$, leading to different morphologies of 3D CuInS$_2$ being produced; that is, a low molar quantity of L-cysteine is not beneficial for the formation of 3D CuInS$_2$, however, the addition of L-cysteine at a high molar quantity would result in the appearance of a heterogeneous crystal.

3.2.1.2 The influence of different solvents. With the synthesized 3D In$_2$S$_3$ as the template, and with the cooperation of additional Cu^{2+}, 3D In$_2$S$_3$ transforms to 3D CuInS$_2$. In this step, the solvent plays an important role. Fig. 5 shows the influence of different solvents on the morphology of 3D CuInS$_2$. Fig. 5a displays CuInS$_2$ synthesized in aqueous solution; huge spheres

with a size of about 5–6 μm could be observed, along with the presence of many fragmentary particles. However, in glycol solvent, smaller spheres with a size of 0.8–1 μm could be seen, which were assembled from many flakes (as shown in Fig. 5b). When CuInS$_2$ was synthesized in DMF solvent (Fig. 5c), the SEM image shows that the products are walnut-shape 3D microspheres with diameters ranging from 400–600 nm, which are constructed from extremely developed hierarchical structures assembled from many interleaving and bending nanosheets. The flakes, aligned along different orientations, connected with each other to form a bunch, ultimately producing pinnacles at the centre of the hierarchical structure. Obviously, a change in solvent normally results in largely different morphologies of the products. DMF, as a strong coordinating solvent, is beneficial to the promotion of a 3D hierarchical structure. In a TEM image (Fig. 5d), particles with a size of about 500 nm could be seen clearly, with some obvious intervals existing between the adjacent nanosheets. The dark centre and pale perimeter of the product (shown in the inset of Fig. 5d) implied that the hierarchical structure is assembled in a compact manner at the centre, with very thin flakes along the perimeter.

3.2.2 Characterization of 3D CuInS$_2$

3.2.2.1 XRD analysis of CuInS$_2$. Fig. 6 shows the XRD pattern of the obtained CuInS$_2$ originating from In$_2$S$_3$, which was synthesized using 4.5 mmol of L-cysteine as the additive. Diffraction peaks at $2\theta = 27.9°$, $32.3°$, $46.4°$ and $55.1°$ could be observed, which were assigned to the (112), (004), (204) or (220) crystal planes of CuInS$_2$ with a chalcopyrite structure ($a = b = 5.523$ Å and $c = 11.133$ Å, JCPDS PCPDFWIN #85-1575).[13b] No impurity phase from In$_2$S$_3$ appeared, indicating that In$_2$S$_3$ transformed into CuInS$_2$ completely.

3.2.2.2 Raman spectrum of CuInS$_2$. As a non-destructive characterization technique, a Raman scattering study could be applied to the analysis of CuInS$_2$ powders prepared by a chemical route, to obtain the best possible crystalline CuInS$_2$ in powder form.[37] Fig. 7 shows the Raman spectrum of a CuInS$_2$ powder sample. It may be observed that there are five peaks at 240, 263, 291, 319 and 340 cm^{-1} from the sample, which were assigned to the E, B2, A1, E and B2 modes of the chalcopyrite phase of CuInS$_2$.[38] The strong peak at 291 cm^{-1} may be assigned

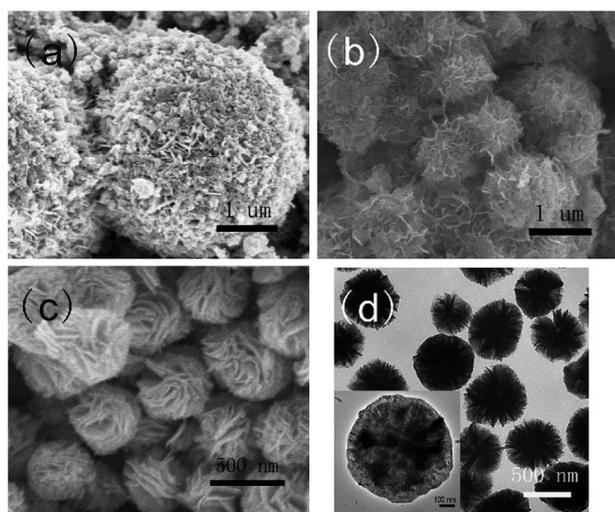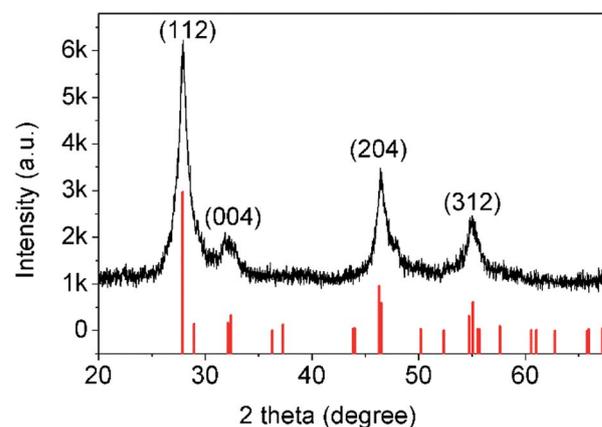**Fig. 5** SEM (a–c) and TEM (d) images of CuInS$_2$ with water (a), glycol (b) and DMF (c, d) as solvents. The inset of (d) is a single particle on a magnified scale.
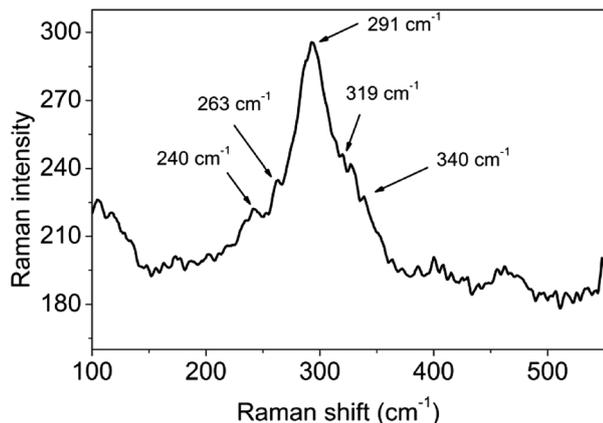

Fig. 6 XRD pattern of the synthesized CuInS$_2$.

Fig. 7 Raman spectrum of the synthesized $CuInS_2$.

to the A1 mode, while the peak at 340 cm^{-1} may be assigned to the B2 mode.[37] The Raman peak at 291 cm^{-1} was fitted to a Gaussian curve and the full-width at half-maximum (FWHM) was estimated to be 40.8 cm^{-1}. Single crystal $CuInS_2$ and almost defect free $CuInS_2$ thin films were reported to have a FWHM of 3.5 and 5 cm^{-1}, respectively.[39] Compared to these values, the FWHM of our sample was much higher, indicating that considerable surface defects existed in the synthesized $CuInS_2$. Clearly, 3D $CuInS_2$ synthesized *via* a solvothermal method could not obtain favorable crystallinity.

3.2.2.3 XPS analysis of $CuInS_2$. Fig. 8 shows XPS spectra of $CuInS_2$. From the survey spectrum (Fig. 8a), we could identify the existence of Cu, In, S, C and O. Similarly to the previous XPS data from In_2S_3, the presence of C and O is probably due to the presence of L-cysteine covering on the product and atmospheric contamination. The core level of the Cu 2p spectrum is split into Cu $2p_{3/2}$ (931.5 eV) and Cu $2p_{1/2}$ (951.3 eV) (Fig. 8b), in accordance with Cu$^+$, but largely different from Cu $2p_{3/2}$ of Cu^{2+} (centred at 942 eV).[40] Obviously, Cu in $CuInS_2$ exists in the form of Cu$^+$; Cu^{2+} as the reactant has been reduced by S^{2-}, which originated from the decomposition of L-cysteine during the reaction. Similarly to the XPS pattern of In_2S_3, there are In $3d_{5/2}$

and In $3d_{3/2}$ peaks at 444.65 eV and 452.2 eV in the 3d spectrum, respectively (Fig. 8c).[28]

Moreover, the peaks at 161.7 eV for Cu–S and 162.8 eV for In–S could be observed in the S 2p core level spectrum (Fig. 8d). They are separated by an energy difference of 1.1 eV, similar to that for $CuInS_2$.[41] The above XPS data agree well with previous results.[42] The quantification results showed a stoichiometric ratio of Cu : In : S of 1 : 1.2 : 2.1, which is very close to that of $CuInS_2$.

3.2.2.4 Absorption spectrum. The UV-vis absorption spectrum of 3D $CuInS_2$ was measured at room temperature in an ethanol dispersion (Fig. 9); typically, a broad shoulder without an obvious peak is visible in the absorption profile with a tail nearly to 900 nm, displaying good light-harvesting properties in the UV-visible range, similar to previous reports.[42b,43] Using the direct band gap method, that is, plotting the squared absorbance *versus* energy and extrapolating to zero (inset of Fig. 9),[44] the band gap of 3D $CuInS_2$ is evaluated to be *ca.* 1.7 eV. Compared to the band gap of 1.5 eV in bulk $CuInS_2$, this is blue-shifted obviously, which originates from the nanostructure existing in 3D $CuInS_2$, confirming the quantum size effect.

3.2.3 Formation mechanism of 3D $CuInS_2$. As mentioned above, the formation of 3D $CuInS_2$ is based on 3D In_2S_3 as the template, while 3D In_2S_3 is formed with the assistance of L-cysteine. Previous reports suggested that In^{3+} and OH$^-$ were firstly bonded to form an $In(OH)_3$ precipitate, then $In(OH)_3$ dissolved after it coordinated with L-cysteine, owing to some groups such as carboxyl, amidogen and sulfydryl existing in L-cysteine,[28] forming a composite between In^{3+} and L-cysteine (an In–L composite), which served as both the indium source and the sulfur source. Then the In–L composite decomposed to form In_2S_3 nuclei, and In_2S_3 grew larger gradually to form In_2S_3 nanoflakes, as the In–L composite decomposed slowly, followed by nanoflakes with different orientations assembling to form flowerlike 3D hierarchical In_2S_3. When the molar quantity of L-cysteine is fairly low, only a small amount of $In(OH)_3$ could coordinate with L-cysteine to form the In–L composite, and the quantity of the composite could not meet the ion quantity demands of 3D In_2S_3 crystal growth after the formation of In_2S_3
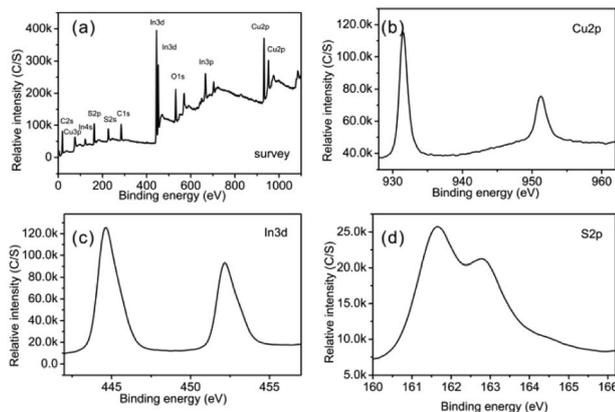

Fig. 8 XPS spectra of the as-synthesized $CuInS_2$: (a) a survey spectrum, (b) a Cu 2p spectrum, (c) an In 3d spectrum, and (d) a S 2p spectrum.

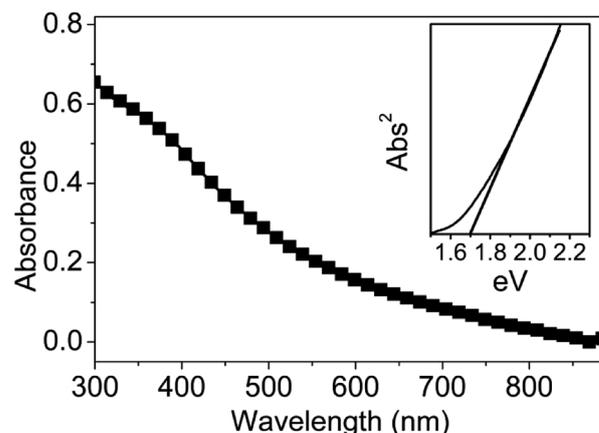**Fig. 9** UV-vis absorption spectrum of 3D $CuInS_2$; the inset is the determination of the band gap using the direct band gap method.

crystal seeds. Large amounts of $In(OH)_3$ and S^{2-} would exist in solution, which are inclined to precipitate quickly, resulting in the formation of some small irregular shaped crystals, instead of hierarchical crystals. When the molar quantity of L-cysteine goes on increasing, more $In(OH)_3$ would coordinate with L-cysteine to form In–L composites, which would release more In^{3+} and S^{2-} after the formation of In_2S_3 nucleus, promoting oriented growth to produce 3D In_2S_3. However, when the molar quantity of L-cysteine is too high, it may result in large amounts of In–L composite decomposing quickly followed by over-fast crystal growth, and the inhomogeneous particles would deposit on large 3D In_2S_3 crystals.

Using 3D In_2S_3 as the template, additional Cu^{2+} and L-cysteine were added to synthesize 3D $CuInS_2$. Cu^{2+} was reduced to Cu^+ by S^{2-} originating from L-cysteine,[45] followed by the combination of 3D In_2S_3 and Cu^+ to form 3D $CuInS_2$. In this step, the solvent plays an important role in the morphology of 3D $CuInS_2$. When the solvent is water, only irregular particles are produced (Fig. 5a). Water is the solvent with weak coordinating abilities; it could not combine Cu^{2+} effectively. Therefore, the additive Cu^{2+} ions were reduced to Cu^+, and lots of Cu^+ would combine with In_2S_3 instantly to form plenty of $CuInS_2$ crystal nuclei and grow quickly, leading to the appearance of irregular particles. However, a glycol solvent displayed strong coordinating abilities, and could combine with Cu^{2+} to form the composite. Initially, some of the composite would be reduced and decomposed to produce Cu^+. As Cu^+ is consumed, that is, to combine with In_2S_3 to form $CuInS_2$, Cu^{2+} would be released from the composite gradually and be reduced, which is beneficial for the formation of the 3D hierarchical structure. Moreover, DMF displayed stronger coordinating abilities, and could combine with Cu^{2+} tightly; only after the consumption of Cu^{2+} almost completely from the solution would it decompose to release Cu^{2+}. Therefore, after the production of the initial $CuInS_2$ nuclei, the slowing release of Cu^{2+} would result in oriented growth to form the large 3D hierarchical structure.

Obviously, in this experiment, L-cysteine displayed a strong tendency to coordinate with In^{3+}, leading to In^{3+} and S^{2-} being released slowly and decreasing the formation rate of In_2S_3, contributing to the formation of 3D In_2S_3. Furthermore, DMF as a strong coordinating solvent could combine with Cu^{2+} which would be reduced to Cu^+. On the basis of 3D In_2S_3, Cu^+ would combine with 3D In_2S_3 slowly, transforming to 3D $CuInS_2$.

3.3 Solar cells

3.3.1 Absorption spectra of MEH–PPV–CuInS$_2$ composite film.
Fig. 10 displays the UV-vis absorption spectra of an MEH–PPV–CuInS$_2$ composite film. In comparison to the 400–600 nm absorption trait of MEH–PPV, originating from the π–π* band,[46] the composite film displays stronger absorbance from 300 nm almost up to 900 nm. This resulted from a complementary absorption contribution from $CuInS_2$ to MEH–PPV. There are no additional absorption peaks, only the single absorption sum of MEH–PPV and $CuInS_2$ in the absorption spectra, indicating that there is hardly any ground-state charge transfer between MEH–PPV and $CuInS_2$.[47]
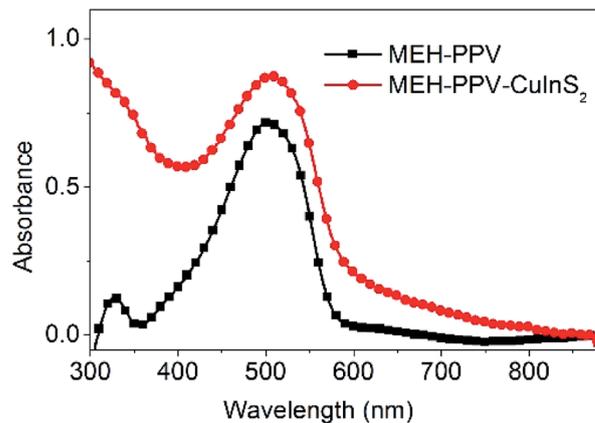
Fig. 10 UV-vis absorption spectra of the composited film.

3.3.2 PL spectra.
Fig. 11 shows PL spectra of the polymer and 3D $CuInS_2$ composite. Compared to the pristine polymer film, the PL spectrum of the composite exhibits a similar emission profile, besides the largely reduced PL intensity, suggesting there exists obvious polymer PL quenching. The PL quenching efficiency (QE) could be obtained by contrasting the maximum PL intensity of the composite with that of the pristine polymer. The results show that the composite obtained a QE of 62.03%, which indicates effective charge transfer from MEH–PPV to $CuInS_2$.[2,48]

3.3.3 Device performance of MEH–PPV/3D CuInS$_2$ solar cells.
Fig. 12 shows the device structure and energy level diagram of an MEH–PPV/3D $CuInS_2$ solar cell. Obviously, the device displayed a typical bulk heterojunction structure, with a mixture of MEH–PPV and 3D $CuInS_2$ as the photoactive layer. From the energy level diagram, it could be clearly observed that MEH–PPV is mainly the electron donor and 3D $CuInS_2$ is the acceptor. Fig. 13 shows the J–V curve of the device under monochromatic illumination at 470 nm with an intensity of 15.85 mW cm^{-2}. The device exhibits a V_{oc} value of 0.401 V, a J_{sc} value of 0.503 mA cm^{-2} and a FF of 0.347, obtaining a PCE of 0.44.

In comparison to our previous devices based on MEH–PPV and $CuInS_2$ quantum dots (QDs),[13a,b] J_{sc} is much higher, which
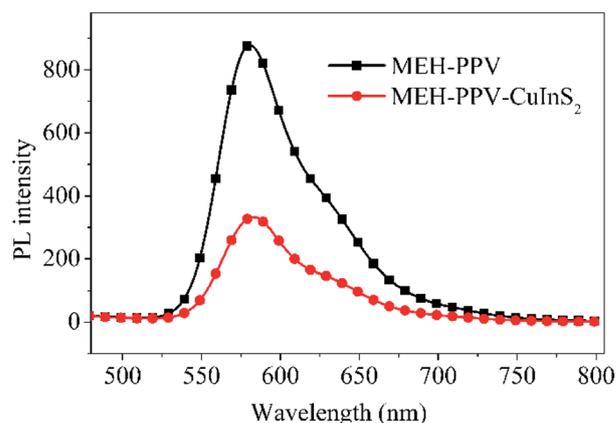
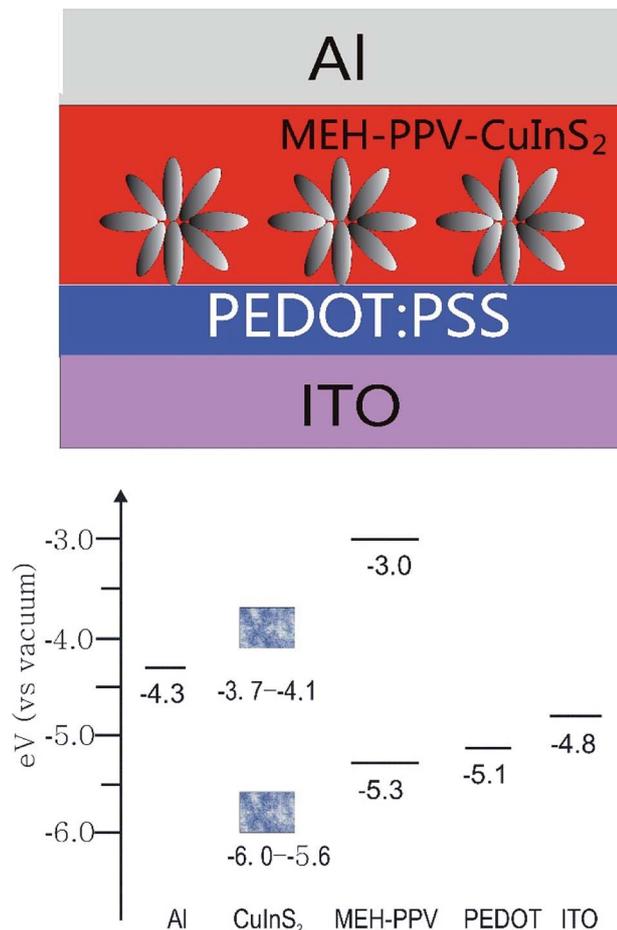**Fig. 11** PL spectra of composited film.

Fig. 12 Device structure and energy level diagram for a MEH–PPV/3D CuInS$_2$ solar cell. The data for ITO, PEDOT, MEH–PPV and Al are obtained by referring to ref. 13a and data for CuInS$_2$ is obtained by referring to ref. 8c.
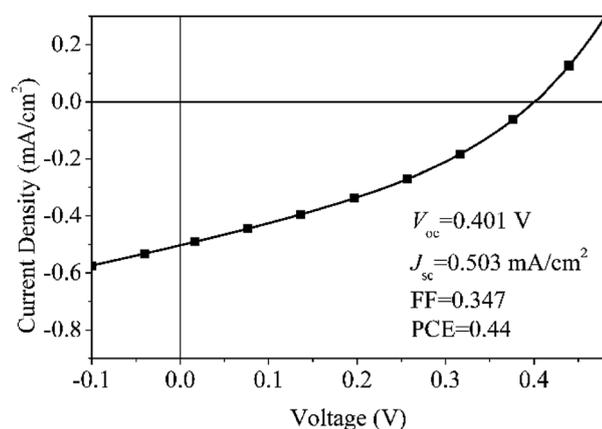

Fig. 13 J–V curve of a MEH–PPV/3D CuInS$_2$ solar cell.

is due to the different electron transport method. In the previous device of MEH–PPV/CuInS$_2$ QDs, QDs were distributed sporadically throughout the conjugated polymer film, making the charge transport *via* a hopping method between energy states, which is easily affected by defect sites existing in the photoactive layer. The presence of defect site would result in the charge recombination and discontinuous transport. Moreover, the randomly distributed MEH–PPV/CuInS$_2$ interface normally leads to incomplete polymer PL quenching, particularly in the region which is more than the exciton diffusion length of the polymer away from the CuInS$_2$ QDs.[49] However, in the present device consisting of MEH–PPV and 3D CuInS$_2$, 3D CuInS$_2$ has a large active surface area, which would have high light scattering capacity.[14] The large surface area and capacious interspaces (as shown in Fig. 5d) in the walnut-shape 3D structure offer more opportunities for the diffusion and mass transportation of MEH–PPV, contributing to the increased light-harvesting ability.[50] On the other hand, the nanosheets in the 3D CuInS$_2$ have very small thickness (only about 10–20 nm), which would promote charge transfer along straight pathways to the electrode, contributing to increased charge transport efficiency.[51] Additionally, the increase in the charge-transfer rates drastically reduces the direct recombination of photo-generated electron–hole pairs, contributing to the higher charge collection efficiency.[51] In conclusion, greater efficient light-harvesting ability, increased charge transport efficiency and the decreased recombination of the photogenerated electron–hole pairs contributed to the higher J_{sc}.

Compared to the previous device,[13a] V_{oc} displayed different results depending on the surface state of 3D CuInS$_2$. V_{oc} is comparable to that of the device based on originally synthesized and untreated QDs, but is lower than that from surface-treated QDs. As we know, in HPSCs, the energy difference between the HOMO level of the donor (D) and the conduction band edge (CB) of the acceptor (A) determines V_{oc}.[52] In these two devices, the same D (MEH–PPV) and A (CuInS$_2$) materials occupy almost the same HOMO and CB positions, therefore, the obviously different V_{oc} may originate from other factors. Actually, it is mainly relevant to observe the quasi-Fermi level energy difference between electrons in the A and holes in the D.[53] V_{oc} in the present device is comparable to that of the previous device containing originally untreated CuInS$_2$ QDs, which is due to the capping molecule L-cysteine covering on the surface of CuInS$_2$ to produce more surface defects (as confirmed from the Raman spectrum), resulting in electrons being more easily trapped and accumulated in the lower quasi-Fermi levels than in the conduction band,[54] leading to a low V_{oc}.

It's noted that FF of the device is rather low. As we know, an important factor influencing the FF is the charge transport properties. According to a previous paper, the hole mobility (μ_h) of MEH–PPV and the electron mobility (μ_e) of CuInS$_2$ are about 10^{-6} cm^2 V^{-1} s^{-1} [55] and 10^1 to 10^2 cm^2 V^{-1} s^{-1};[56] the larger difference between μ_e and μ_h would lead to the charge transport rate imbalance,[57] contributing to the poor FF. Similar phenomena have been reported in a comparison of the device performance between PPV/PCBM device and P3HT/PCBM system. The μ_h of PPV derivative (10^{-5} to 10^{-6} cm^2 V^{-1} s^{-1}) is two or three orders of magnitude less than the μ_e of PCBM phase (10^{-3} cm^2 V^{-1} s^{-1}),[58] but the μ_h of P3HT (10^{-4} cm^2 V^{-1} s^{-1}) is comparable to the μ_e of PCBM (10^{-3} cm^2 V^{-1} s^{-1}). As a result, in most devices, FF in PPV/PCBM device[59] is much lower than that in P3HT/PCBM device.[60] Additionally, the

incompatible D/A interface may also result in the low FF. Normally, an inorganic material such as $CuInS_2$ is hydrophilic, while an organic material such as MEH–PPV is hydrophobic, which would lead to serious incompatibility at the inorganic/organic interface, not favouring charge transfer between MEH–PPV and $CuInS_2$. Moreover, the large amount of capping molecules covering on the surface of $CuInS_2$ would impede electron transport, and the presence of considerable surface defects (as confirmed in the Raman spectrum) would cause much easier charge recombination of electron–hole pairs.[61] All the above factors may result in the poor FF for the MEH–PPV/3D $CuInS_2$ device.

In conclusion, we fabricate a MEH–PPV/3D $CuInS_2$ device and obtain a PCE of 0.4%. The PCE is rather low compared to other PSCs with ZnO,[2] TiO_2,[3] or CdSe[4a] as the acceptor, probably due to the poor crystallinity of $CuInS_2$ synthesized *via* solvothermal methods. However, it is much higher than previous reports based on similarly structured devices based on $CuInS_2$ nanoparticles,[8b,c,13a,b] suggesting that 3D $CuInS_2$ is a promising structure when applied in HPSCs. It could be anticipated that, to obtain photovoltaic devices based on 3D $CuInS_2$ with a higher power conversion efficiency, it is necessary to optimize the synthesis method to obtain $CuInS_2$ with an ideal surface structure and better crystallinity, to apply surface modification to the inorganic and organic components, and to utilize Li salt doping to increase the hole mobility of MEH–PPV.

4.   Conclusions

3D hierarchical micro/nanostructured $CuInS_2$ was synthesized with pre-synthesized 3D In_2S_3 as the template. In the synthesis of In_2S_3, we found that 3D uniform flower-like β-In_2S_3 was synthesized successfully with the assistance of L-cysteine. Based on 3D In_2S_3, 3D $CuInS_2$ could be synthesized successfully. The molar quantity of L-cysteine and the used solvent had important influences on the morphology of 3D $CuInS_2$. When In_2S_3 was synthesized with 4.5 mmol L-cysteine as the additive, with the cooperation of Cu^{2+} in DMF solution, walnut-shape 3D $CuInS_2$ with a chalcopyrite structure was formed. We consider that the formation of 3D $CuInS_2$ may originate from the strong coordinating effects of L-cysteine and DMF, which would lead to slow ion release and oriented crystal growth. $CuInS_2$ displayed a wide absorption range in the UV-vis spectrum, and it could increase the absorption ability of a MEH–PPV–$CuInS_2$ composite film and quench the PL of MEH–PPV effectively. As a result, 3D $CuInS_2$ was used to fabricate MEH–PPV/3D $CuInS_2$ solar cells, obtaining a PCE of 0.4%. The high J_{sc} value may result from the hierarchical structure, with a large active surface area and capacious interspaces, being beneficial to the penetration of MEH–PPV, and it could afford an effective path for electron transport and collection, while the low V_{oc} may originate from plenty of capping molecules covering on the surface of $CuInS_2$. The successful fabrication of MEH–PPV/3D $CuInS_2$ solar cells suggests that 3D $CuInS_2$ may be an effective electron acceptor for efficient HPSCs in the future.

Notes and references

1 (a) N. S. Sariciftci, L. Smilowitz and F. W. A. J. Heeger, *Science*, 1992, **258**, 1474; (b) G. Yu, J. Gao, J. C. Hummelen, F. Wudl and A. J. Heeger, *Science*, 1995, **270**, 1789.

2 W. J. E. Beek, M. M. Wienk and R. A. J. Janssen, *Adv. Funct. Mater.*, 2006, **16**, 1112.

3 P. A. v. Hal, M. M. Wienk, J. M. Kroon, W. J. H. Verhees, L. H. Slooff, W. J. H. v. Gennip, P. Jonkheijm and R. A. J. Janssen, *Adv. Mater.*, 2003, **15**, 118.

4 (a) W. U. Huynh, J. J. Dittmer and A. P. Alivisatos, *Science*, 2002, **295**, 2425; (b) A. P. Alivisatos, *Science*, 1996, **271**, 933.

5 N. C. Greenham, X. Peng and A. P. Alivisatos, *Phys. Rev. B: Condens. Matter Mater. Phys.*, 1996, **54**, 17628.

6 (a) S. A. McDonald, G. Konstantatos, S. Zhang, P. W. Cyr, E. J. D. Klem, L. Levina and E. H. Sargent, *Nat. Mater.*, 2005, **4**, 138; (b) S. Günes, K. P. Fritz, H. Neugebauer, N. S. Sariciftci, S. Kumar and G. D. Scholes, *Sol. Energy Mater. Sol. Cells*, 2007, **91**, 420.

7 D. Cui, J. Xu, T. Zhu, G. Paradee, S. Ashok and M. Gerhold, *Appl. Phys. Lett.*, 2006, **88**, 183111.

8 (a) E. Arici, D. Meissner and N. S. Sariciftci, *Encyclopedia of Nanoscience and Nanotechnology*, ed. H. S. Nalwa, 2004, vol. 3, p. 929; (b) M. Piber, T. Rath, T. Grieber, G. Trimmel, F. Stelzer and D. Meissner, *2006 IEEE 4th World Conference on Photovoltaic Energy Conversion*, 2006, vol. 1, p. 247; (c) E. Arici, N. S. Sariciftci and D. Meissner, *Adv. Funct. Mater.*, 2003, **13**, 165.

9 (a) M. A. Green, K. Emery, D. L. King, S. Igari and W. Warta, *Prog. Photovoltaics*, 2002, **10**, 355; (b) H. J. Lewerenz, H. Goslowsky, K.-D. Husemann and S. Fiechter, *Nature*, 1986, **321**, 687.

10 B. Tell, J. L. Shay and H. M. Kasper, *Phys. Rev. B: Solid State*, 1971, **4**, 2463.

11 (a) M. Afzaala and P. O'Brien, *J. Mater. Chem.*, 2006, **16**, 1297; (b) H. J. Lewerenz, *Sol. Energy Mater. Sol. Cells*, 2004, **83**, 395; (c) R. Klenk, J. Klaer, R. Scheer, M. C. Lux-Steiner, I. Luck, N. Meyer and U. Rühle, *Thin Solid Films*, 2005, **480–481**, 509.

12 D. C. Look and J. C. Manthuruthil, *J. Phys. Chem. Solids*, 1976, **37**, 173.

13 (a) W. Yue, S. Han, R. Peng, W. Shen, H. Geng, F. Wu, S. Tao and M. Wang, *J. Mater. Chem.*, 2010, **20**, 7570; (b) W. Yue, M. Lan, G. Zhang, W. Sun, S. Wang and G. Nie, *Mater. Sci. Semicond. Process.*, 2014, **24**, 117; (c) W. Yue, F. Wu, C. Liu, Z. Qiu, Q. Cui, H. Zhang, F. Gao, W. Shen, Q. Qiao and M. Wang, *Sol. Energy Mater. Sol. Cells*, 2013, **114**, 43; (d)

W. Yue, C. Liu, Z. Qiu and M. Wang, *Sol. Energy*, 2015, **113**, 358.

14 F. Shao, J. Sun, L. Gao, S. Yang and J. Luo, *ACS Appl. Mater. Interfaces*, 2011, **3**, 2148.

15 L. Yu, Z. Li, Y. Liu, F. Cheng and S. Sun, *Appl. Surf. Sci.*, 2014, **305**, 359.

16 M. J. Bierman and S. Jin, *Energy Environ. Sci.*, 2009, **2**, 1050.

17 (a) M. Liu, G. Li and X. Chen, *ACS Appl. Mater. Interfaces*, 2014, **6**, 2604; (b) C. Wen, X. Weidong, W. Juanjuan, W. Xiaoming, Z. Jiasong and L. Lijun, *Mater. Lett.*, 2009, **63**, 2495; (c) S. Peng, F. Cheng, J. Liang, Z. Tao and J. Chen, *J. Alloys Compd.*, 2009, **481**, 786.

18 (a) Q. A. Akkerman, A. Genovese, C. George, M. Prato, I. Moreels, A. Casu, S. Marras, A. Curcio, A. Scarpellini, T. Pellegrino, L. Manna and V. Lesnya, *ACS Nano*, 2015, **9**, 521; (b) W. van der Stam, A. C. Berends, F. T. Rabouw, T. Willhammar, X. Ke, J. D. Meeldijk, S. Bals and C. de Mello Donega, *Chem. Mater.*, 2015, **27**, 621; (c) T. Kuzuya, Y. Hamanaka, K. Itoh, T. Kino, K. Sumiyama, Y. Fukunaka and S. Hirai, *J. Colloid Interface Sci.*, 2012, **388**, 137; (d) V. Lesnyak, C. George, A. Genovese, M. Prato, A. Casu, S. Ayyappan, A. Scarpellini and L. Manna, *ACS Nano*, 2014, **8**, 8407.

19 (a) L. Zheng, Y. Xu, Y. Song, C. Wu, M. Zhang and Y. Xie, *Inorg. Chem.*, 2009, **48**, 4003; (b) D. Wu, J. Duan, C. Zhang, K. Guo and H. Zhu, *J. Phys. Chem. C*, 2013, **117**, 9121.

20 H. Migge and J. Grzanna, *J. Mater. Res.*, 1994, **9**, 125.

21 S. Lei, C. Wang, L. Liu, D. Guo, C. Wang, Q. Tang, B. Cheng, Y. Xiao and L. Zhou, *Chem. Mater.*, 2013, **25**, 2991.

22 B. Chen, S. Chang, D. Li, L. Chen, Y. Wang, T. Chen, B. Zou, H. Zhong and A. L. Rogach, *Chem. Mater.*, 2015, **27**, 5949.

23 R. Diehl and R. Nitsche, *J. Cryst. Growth*, 1975, **28**, 306.

24 Q. Lu, F. Gao and S. Komarneni, *J. Am. Chem. Soc.*, 2004, **126**, 54.

25 M. Valodkar, A. Pal and S. Thakore, *J. Alloys Compd.*, 2011, **509**, 523.

26 F. Chen, R. Zhou, L. Yang, M. Shi, G. Wu, M. Wang and H. Chen, *J. Phys. Chem. C*, 2008, **112**, 13457.

27 F. Gao, Q. Lu, X. Meng and S. Komarneni, *J. Phys. Chem. C*, 2008, **112**, 13359.

28 L.-Y. Chen, Z.-D. Zhang and W.-Z. Wang, *J. Phys. Chem. C*, 2008, **112**, 4117.

29 F. Zuo, F. Yan, B. Zhang, Y. Zhao and Y. Xie, *J. Phys. Chem. C*, 2008, **112**, 2831.

30 J. Jiang, R. Yu, R. Yi, W. Qin, G. Qiu and X. Liu, *J. Alloys Compd.*, 2010, **493**, 529.

31 J. Pan, S. Xiong, B. Xi, J. Li, J. Li, H. Zhou and Y. Qian, *Eur. J. Inorg. Chem.*, 2009, 5302.

32 J. Xiang, H. Cao, Q. Wu, S. Zhang, X. Zhang and A. A. R. Watt, *J. Phys. Chem. C*, 2008, **112**, 3580.

33 S. Xiong, B. Xi, C. Wang, D. Xu, X. Feng, Z. Zhu and Y. Qian, *Adv. Funct. Mater.*, 2007, **17**, 2728.

34 S. Xiong, B. Xi, C. Wang, G. Zou, L. Fei, W. Wang and Y. Qian, *Chem*, 2007, **13**, 3076.

35 X. Fu, X. Wang, Z. Chen, Z. Zhang, Z. Li, D. Y. C. Leung, L. Wu and X. Fu, *Appl. Catal., B*, 2010, **95**, 393.

36 (a) N. Revathi, P. Prathap, Y. P. V. Subbaiah and K. T. Ramakrishna Reddy, *J. Phys. D: Appl. Phys.*, 2008, **41**, 155404; (b) S.-H. Yu, L. Shu, Y.-S. Wu, J. Yang, Y. Xie and Y.-T. Qian, *J. Am. Ceram. Soc.*, 1999, **82**, 457.

37 P. Guha, D. Das, A. B. Maity, D. Ganguli and S. Chaudhuri, *Sol. Energy Mater. Sol. Cells*, 2003, **80**, 115.

38 K. Das, S. K. Panda, S. Gorai, P. Mishra and S. Chaudhuri, *Mater. Res. Bull.*, 2008, **43**, 2742.

39 J. Álvarez-García, J. Marcos-Ruzafa, A. Pérez-Rodríguez, A. Romano-Rodríguez, J. R. Morante and R. Scheer, *Thin Solid Films*, 2000, **361–362**, 208.

40 (a) J. Llanos, A. Buljan, C. Mujica and R. Ramfrez, *J. Alloys Compd.*, 1996, **234**, 40; (b) L. D. Partain, R. A. Schneider, L. F. Donaghey and P. S. McLeod, *J. Appl. Phys.*, 1985, **57**, 5056.

41 J. F. Moulder, W. F. Stickle, P. E. Sobol and K. Bomben, *X-Ray Data Booklet*, Copyright 1992 by Perkin-Elmer Corp.: Physical Electronic Division, 1992.

42 (a) J. Xiao, Y. Xie, R. Tang and Y. Qian, *J. Solid State Chem.*, 2001, **161**, 179; (b) D. Pan, L. An, Z. Sun, W. Hou, Y. Yang, Z. Yang and Y. Lu, *J. Am. Chem. Soc.*, 2008, **130**, 5620.

43 (a) H. Nakamura, W. Kato, M. Uehara, K. Nose, T. Omata, S. Otsuka-Yao-Matsuo, M. Miyazaki and H. Maeda, *Chem. Mater.*, 2006, **18**, 3330; (b) H. Zhong, Y. Zhou, M. Ye, Y. He, J. Ye, C. He, C. Yang and Y. Li, *Chem. Mater.*, 2008, **20**, 6434.

44 Q. Guo, S. J. Kim, M. Kar, W. N. Shafarman, R. W. Birkmire, E. A. Stach, R. Agrawal and H. W. Hillhouse, *Nano Lett.*, 2008, **8**, 2982.

45 S. Han, M. Kong, Y. Guo and M. Wang, *Mater. Lett.*, 2009, **63**, 1192.

46 S.-S. Kim, J. Jo, C. Chun, J.-C. Hong and D.-Y. Kim, *J. Photochem. Photobiol., A*, 2007, **188**, 364.

47 N. C. Greenham, X. Peng and A. P. Alivisatos, *Phys. Rev. B: Condens. Matter Mater. Phys.*, 1996, **54**, 17628.

48 (a) Y.-Y. Lin, T.-H. Chu, C.-W. Chen and W.-F. Su, *Appl. Phys. Lett.*, 2008, **92**, 053312; (b) Y. Y. Lin, T. H. Chu, S. S. Li, C. H. Chuang, C. H. Chang, W. F. Su, C. P. Chang, M. W. Chu and C. W. Chen, *J. Am. Chem. Soc.*, 2009, **131**, 3644; (c) J. H. Warner, A. R. Watt, E. Thomsen, N. Heckenberg, P. Meredith and H. Rubinsztein-Dunlop, *J. Phys. Chem. B*, 2005, **109**, 9001.

49 K. M. Coakley and M. D. McGehee, *Chem. Mater.*, 2004, **16**, 4533.

50 L. Feng, J. Jia, Y. Fang, X. Zhou and Y. Lin, *Electrochim. Acta*, 2013, **87**, 629.

51 B. Li and Y. Wang, *J. Phys. Chem. C*, 2010, **114**, 890.

52 (a) S. Günes, H. Neugebauer and N. S. Sariciftci, *Chem. Rev.*, 2007, **107**, 1324; (b) M. Skompska, *Synth. Met.*, 2010, **160**, 1; (c) T. Xu and Q. Qiao, *Energy Environ. Sci.*, 2011, **4**, 2700; (d) D. C. Olson, S. E. Shaheen, M. S. White, W. J. Mitchell, M. F. A. M. van Hest, R. T. Collins and D. S. Ginley, *Adv. Funct. Mater.*, 2007, **17**, 264; (e) M. C. Scharber, D. Mühlbacher, M. Koppe, P. Denk, C. Waldauf, A. J. Heeger and C. J. Brabec, *Adv. Mater.*, 2006, **18**, 789.

53 (a) Y.-Y. Lin, T.-H. Chu, S.-S. Li, C.-H. Chuang, C.-H. Chang, W.-F. Su, C.-P. Chang, M.-W. Chu and C.-W. Chen, *J. Am. Chem. Soc.*, 2009, **131**, 3644; (b) J. Bisquert and G. Garcia-

Belmonte, *J. Phys. Chem. Lett.*, 2011, **2**, 1950; (*c*) M. M. Lee, J. Teuscher, T. Miyasaka, T. N. Murakami and H. J. Snaith, *Science*, 2012, **338**, 643.

54 (*a*) K. Schwarzburg and F. Willig, *Appl. Phys. Lett.*, 1991, **58**, 2520; (*b*) G. Boschloo and A. Hagfeldt, *J. Phys. Chem. B*, 2005, **109**, 12093.

55 (*a*) Q. Shi, Y. Hou, J. Lu, H. Jin, Y. Li, Y. Li, X. Sun and J. Liu, *Chem. Phys. Lett.*, 2006, **425**, 75; (*b*) M. H. Li, H.-L. Chen, Y.-F. Huang, W.-T. Chuang, Y.-R. Chen, H.-S. Tsai, O. A. Semenikhin and J. D. White, *Chem. Phys. Lett.*, 2011, **505**, 100.

56 (*a*) L. L. Kazmerski, M. S. Ayyagari and G. A. Sanborn, *J. Appl. Phys.*, 1975, **46**, 4865; (*b*) Y. L. Wu and H. Y. Lin, *Thin Solid Films*, 1989, **168**, 113.

57 D. Gupta, S. Mukhopadhyay and K. S. Narayan, *Sol. Energy Mater. Sol. Cells*, 2010, **94**, 1309.

58 V. D. Mihailetchi, J. Wildeman and P. W. Blom, *Phys. Rev. Lett.*, 2005, **94**, 126602.

59 (*a*) M. T. Rispens, A. Meetsma, R. Rittberger, C. J. Brabec, N. S. Sariciftci and J. C. Hummelen, *Chem. Commun.*, 2003, **17**, 2116; (*b*) S. E. Shaheen, C. J. Brabec, N. S. Sariciftci, F. Padinger, T. Fromherz and J. C. Hummelen, *Appl. Phys. Lett.*, 2001, **78**, 841; (*c*) T. Munters, T. Martens, L. Goris, V. Vrindts, J. Manca, L. Lutsen, W. D. Ceuninck, D. Vanderzande, L. D. Schepper, J. Gelan, N. S. Sariciftci and C. J. Brabec, *Thin Solid Films*, 2002, **403–404**, 247.

60 G. Li, V. Shrotriya, J. Huang, Y. Yao, T. Moriarty, K. Emery and Y. Yang, *Nat. Mater.*, 2005, **4**, 864.

61 (*a*) A. Moliton and J.-M. Nunzi, *Polym. Int.*, 2006, **55**, 583; (*b*) W. J. Potscavage Jr, A. Sharma and B. Kippelen, *Acc. Chem. Res.*, 2009, **42**, 1758.